Proceedings of the World Congress on New Technologies (NewTech 2015)
Barcelona, Spain – July 15 - 17, 2015
Paper No. 319

Numerical Analysis In Short-Pulse Laser Heating Of Metals Based On The Dual-Phase-Lag Model Of Heat Conduction

Haw-Long Lee, Win-Jin Chang, Yu-Ching Yang
Department of Mechanical Engineering /Kun Shan University,
No.195, Kunda Rd., Yong Kang Dist., Tainan City 710-03, Taiwan (R.O.C.)
hawlong@mail.ksu.edu.tw;changwj@msil/ksu.edu.tw;
ycyang@mail.ksu.edu.tw

Abstract **-**In this study, an efficient numerical scheme is applied to investigate the heat transfer in a thin metal film exposed to short-pulse laser heating based on the dual-phase-lag (DPL) model. The scheme involves the hybrid application of the Laplace transform and control volume methods in conjunction with hyperbolic shape functions. The transformed nodal temperatures are inverted to the physical quantities by using numerical inversion of the Laplace transform. Comparison between the numerical results and the analytic solution for a short-pulse laser heating evidences the accuracy of the present numerical results. Effect of different phase lags values of the heat flux and the temperature gradient on the behavior of heat transfer is also investigated.

Keywords**:** Non-Fourier heat transfer/Dual-phase-lag/Short-pulse laser heating/Hybrid method

1. Introduction

The advancement of micro- or nano-electromechanical systems (MEMS/NEMS) has made various devices perform advanced functions with more compact sizes. Meanwhile, due to the development of short-pulse laser technologies, laser micro-machining, laser pattering, and laser hardening have been applied in the processes of making such electromechanical devices [1]. Short-pulse lasers produce a small heat affected zone and a small recast layer on the machined surface by causing material vaporization through high peak power and shorter interaction time [2]. In the applications of metal processing, short-pulse laser heating of metals involves deposition of radiation energy on electrons, resulting in energy increase in electrons; energy is transferred to lattice through electron-lattice interaction and propagates through media.

To consider the effect of micro-structural interactions on the fast-transient process of heat transport, the dual-phase-lag model accounts for both the temporal and the spatial effects of heat transfer in one-temperature formulation and takes the form [3]:

$$q(r,t+\tau_q) = -k\nabla T(r,t+\tau_T)\,, \tag{1}$$

where T is the temperature, k the heat conductivity, q the heat flux, t the time, and r the space variable. τ_q is the phase lag of the heat flux, and τ_T is the phase lag of the temperature gradient. The heat flux precedes the temperature gradient for $\tau_q < \tau_T$. On the other hand, the temperature gradient precedes the heat flux for $\tau_q < \tau_T$. With the DPL model, not only the temperature gradient can precede the heat flux, but also the heat flux may precede the temperature gradient.

The physical meanings of the DPL model are shown by the experimental results in [4]. In addition, there have been various heat transfer problems described by the DPL model. Ordóñez-Miranda and Alvarado-Gil [5] investigated the one-dimensional thermal wave transport in a semi-infinite medium and obtained the formulas to determine the difference of the time delays as well as other thermal properties of the semi-infinite layer. Liu and Chen [6] interpreted the non-Fourier thermal behavior in hyperthermia

treatment for biological tissue. The comparisons of temperature increase history among the calculated results, the values from the classical bio-heat transfer equation, and the experimental data are made for various measurement locations.

In this study, the problem of short-pulse laser heating on a thin metal film using the DPL model with constant phase lags is analyzed with a hybrid. First, the problem is formulated using the DPL model in general form. Then Laplace transform method is adopted to remove the time-dependent terms from the governing equations. The transformed equations are further discretized by using the control volume method, and a shape function within the control volume is derived from the associated homogeneous equation of the transformed equation. Finally, the transformed nodal temperatures are inverted to the physical quantities by using numerical inversion of the Laplace transform. Comparison between the numerical results and the analytic solution is made to examine the accuracy of the present numerical results. Effect of different phase lag values of the heat flux and the temperature gradient on the behavior of heat transfer is also investigated in this work.

2. Physical Model And Mathmatical Formulation

The problem geometry in this study is simply a thin metal film exposed to a short-laser heat pulse at the front surface (left boundary) [7], as shown in Fig. 1. In a local energy balance, the one-dimensional energy equation of the present problem is given as [7]:

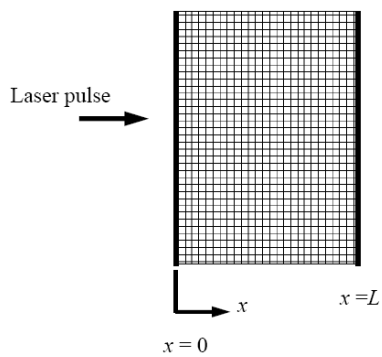

Fig. 1. Geometry and coordinate system

$$-\frac{\partial q(x,t)}{\partial x}+g(x,t)=\rho c\frac{\partial T(x,t)}{\partial t}, \tag{2}$$

where q is the heat flux, ρ the density, and c the specific heat. The source term $g(x,t)$ is the laser energy absorption rate, given in general form as:

$$g(x,t)=g_0F(x)G(t), \tag{3}$$

where g_0 is the intensity of the laser absorption and is a constant, $G(t)$ is the light intensity of the laser beam, and

$$F(x)=e^{-x/\delta}, \tag{4}$$

with δ being the laser penetration depth. To accommodate the micro-structural effect, the DPL model suggested by Tzou [3] is applied to the heat flux equation. This leads to the linear version of the DPL model expressed as:

$$q(x,t)+\tau_q \frac{\partial q(x,t)}{\partial t} = -k\frac{\partial T(x,t)}{\partial x} - k\tau_T \frac{\partial^2 T(x,t)}{\partial t \partial x} \ . \tag{5}$$

By taking the Laplace transform of Eqs. (2) and (5) with s as the Laplace transform parameter gives:

$$-\frac{\mathrm{d}q(x,s)}{\mathrm{d}x} + \bar{g}(x,s) = \rho c s \bar{T}(x,s) - \rho c T_0(x) \ , \tag{6}$$

$$\bar{q}(x,s) - Hq_0(x) = -U\frac{\mathrm{d}\bar{T}(x,s)}{\mathrm{d}x} + W\frac{\mathrm{d}T_0(x)}{\mathrm{d}x} \ , \tag{7}$$

where T_0 is the initial temperature, q_0 is the initial flux, the bar "–" indicates the Laplace transform of the function, and

$$\bar{g}(x,s) = g_0 F(x)\bar{G}(s) \ , \quad H = \frac{\tau_q}{1+\tau_q s} \ , \quad U = \frac{k(1+\tau_T s)}{1+\tau_q s} \ , \quad W = \frac{k\tau_T}{1+\tau_q s} \ . \tag{8}$$

Differentiating Eq. (7) with x and substituting the result in Eq. (6) gives:

$$\frac{\mathrm{d}^2\bar{T}}{\mathrm{d}x^2} - \lambda^2\bar{T} - \frac{W}{U}\frac{\mathrm{d}^2 T_0}{\mathrm{d}x^2} + \frac{\rho c}{U}T_0 - \frac{H}{U}\frac{\mathrm{d}q_0}{\mathrm{d}x} + \frac{1}{U}\bar{g} = 0 \ , \tag{9}$$

where

$$\lambda = \sqrt{\frac{\rho c s(1+\tau_q s)}{k(1+\tau_T s)}} \ . \tag{10}$$

Next, define the reduced temperature $\theta(x,t)$ as:

$$\theta(x,t) = T(x,t) - T(x,0) = T(x,t) - T_0(x) \ . \tag{11}$$

Then, Eq. (9) can be rewritten as:

$$\frac{\mathrm{d}^2\bar{\theta}}{\mathrm{d}x^2} - \lambda^2\bar{\theta} = (\frac{W}{U} - \frac{1}{s})\frac{\mathrm{d}^2 T_0}{\mathrm{d}x^2} + \frac{H}{U}\frac{\mathrm{d}q_0}{\mathrm{d}x} - \frac{1}{U}\bar{g} \ . \tag{12}$$

The above equations are solved with the following initial and boundary conditions:

$$T(x,0) = T_0(x) = T_\infty = \text{const} \ , \quad \frac{\partial T(x,0)}{\partial t} = 0 \ . \tag{13}$$

Substituting Eq. (13) in Eq. (2) results in:

$$q(x,0) = -\delta g_0 F(x) G(0) = q_0(x) \ , \tag{14}$$

then the initial heat flux distribution can be found by integrating Eq. (14):

$$q(x,0) = -\delta g_0 F(x) G(0) = q_0(x) \ . \tag{15}$$

The nonzero initial heat flux distribution associated with a constant initial temperature (i.e., zero initial temperature gradient), as given by Eqs. (13) and (15), are physically meaningful within the framework of the DPL model only when $\tau_q < \tau_T$ where the temperature gradient lags behind the heat flux, which is indeed the case for metals in general. However, for $\tau_q \geq \tau_T$, the heat flux lags behind the temperature gradient and a nonzero initial heat flux distribution associated with an initial zero temperature gradient is physically not possible.

The boundary conditions used in Ref. [3] assuming negligible heat losses at the boundaries:

$$\frac{\partial T(0,t)}{\partial x} = \frac{\partial T(L,t)}{\partial x} = 0\,, \tag{16}$$

or in the Laplace transform domain:

$$\frac{\mathrm{d}\bar{\theta}(0,s)}{\mathrm{d}x} = \frac{\mathrm{d}\bar{\theta}(L,s)}{\mathrm{d}x} = 0\,. \tag{17}$$

In this work, we use the same boundary conditions (Eqs. (16) and (17)) used in Ref. [3]. The governing equation (Eq. (12)) with the above conditions is reduced to:

$$\frac{\mathrm{d}^2\bar{\theta}}{\mathrm{d}x^2} - \lambda^2\bar{\theta} = \frac{H}{U}\frac{\mathrm{d}q_0}{\mathrm{d}x} - \frac{1}{U}\bar{g}\,. \tag{18}$$

Substituting Eq. (15) in Eq. (18) gives rise to:

$$\frac{\mathrm{d}^2\bar{\theta}}{\mathrm{d}x^2} - \lambda^2\bar{\theta} = \gamma F(x)\,, \tag{19}$$

where

$$\gamma = \frac{g_0[HG(0) - \bar{G}]}{U}\,. \tag{20}$$

In this study, the laser heat pulse used in Ref. [7] is adopted and is expressed as:

$$g(x,t) = \frac{2}{\sqrt{\pi/\ln(2)}} J\left(\frac{1-R}{t_p\delta}\right) e^{-x/\delta} e^{-a|t-2t_p|/t_p}\,, \tag{21}$$

where R is the reflectivity of the surface layer, J is the laser fluence, δ is the laser penetration depth, t_p is the Laser pulse full-width-at-half-maximum (FWHM) duration, and a is a constant parameter. Comparing Eq. (21) with Eq. (3) yields:

$$g_0 = \frac{2}{\sqrt{\pi/\ln(2)}} J\left(\frac{1-R}{t_p\delta}\right), \tag{22}$$

$$G(t) = e^{-a|t-2t_p|/t_p}\,, \tag{23}$$

and

$$\bar{G}(s)=\int_0^{\infty} \mathrm{e}^{-st} G(t)dt = t_p[\frac{e^{-2a}-e^{-2st_p}}{st_p-a}+\frac{e^{-2st_p}}{st_p+a}] \ . \tag{24}$$

3. Numerical Method

Under the present framework, the whole space domain is divided into several sub-space domains, as shown in Fig. 2. This facilitates Eq. (19) to be discretized by using a control volume formulation. Integrating of Eq. (19) over the control volume $\Omega=[x_i-l/2, x_i+l/2]$ for the ith interior node yields [8]:

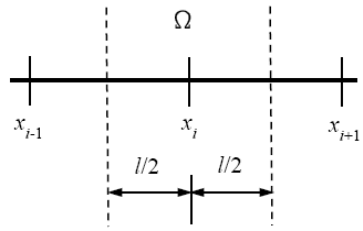

Fig. 2. Schematic diagram of the control volume

$$\int_{x_i-l/2}^{x_i+l/2}[\frac{\mathrm{d}^2\bar{\theta}}{\mathrm{d}x^2}-\lambda^2\bar{\theta}-\gamma F(x)]\mathrm{d}x=0 \ , \tag{25}$$

where l is the distance between two consecutive nodes, and $x_i+l/2=(x_i+x_{i+1})/2$. Then Eq. (25) can further be expressed as:

$$\left.\frac{\mathrm{d}\bar{\theta}}{\mathrm{d}x}\right|_{x_i+l/2}-\left.\frac{\mathrm{d}\bar{\theta}}{\mathrm{d}x}\right|_{x_i-l/2}-\lambda^2\int_{x_i-l/2}^{x_i+l/2}\bar{\theta}dx-\gamma\int_{x_i-l/2}^{x_i+l/2}F(x)\mathrm{d}x=0 \tag{26}$$

In each control volume, the transformed temperature $\bar{\theta}(x,s)$ is approximated in terms of the nodal temperatures and suitable shape functions, as illustrated by Liu et al. [9]. The shape function within the control volume is derived from the associated homogeneous equation of the transformed equation. The use of hyperbolic shape functions can accurately solve the DPL heat conduction problems. Thus, in the present study, the transformed temperatures are approximated by [9]:

$$\bar{\theta}(x,s)=\frac{1}{\sinh(\lambda l)}[\sinh(\lambda(x_i-x))\bar{\theta}_{i-1}+\sinh(\lambda(x-x_i+l))\bar{\theta}_i], \text{ for } x\in[x_i-l,x_i] \ , \tag{27}$$

$$\bar{\theta}(x,s)=\frac{1}{\sinh(\lambda l)}[\sinh(\lambda(x_i+l-x))\bar{\theta}_i+\sinh(\lambda(x-x_i))\bar{\theta}_{i+1}], \text{ for } x\in[x_i,x_i+l] \ . \tag{28}$$

Substituting Eqs. (27) and (28) into Eq. (26) leads to the following discretized form of Eq. (26):

$$A_i\bar{\theta}_{i-1}+B_i\bar{\theta}_i+C_i\bar{\theta}_{i+1}=f_i \ , \text{ for } \ i=2,3,...,n-1, \tag{29}$$

where n is the total node number and

$$A_i=1, \ \ B_i=-2\cosh(\lambda l), \ C_i=1 \text{ ,and } \ f_i=\frac{\sinh(\lambda l)}{\lambda}\cdot 2\delta\gamma e^{-x_i/\delta}\cdot\sinh(l/2\delta) \ . \tag{30}$$

The rearrangement of Eq. (29) in conjunction with the prescribed boundary conditions of Eq. (17)

yields the following vector-matrix equation:

$$[M]\{\bar{\theta}\}=\{f\}. \tag{31}$$

Finally, the inverse Laplace transform of the nodal temperatures $\{\bar{\theta}\}$in Eq. (31) is completed by the application of the Fourier series technique used in our previous work [10].

4. Results And Discussion

The same parameters used in Ref. [7] to theoretically predict the reflectivity change of a thin gold film are used in this work:

$$J = 13.4\ \mathrm{J\,m^{-2}},\ \delta = 15.3\times10^{-9}\ \mathrm{m},\ a = 1.992,\ t_p = 100\times10^{-15}\ \mathrm{s},\ R = 0.93.$$

In addition, we consider the gold film with the following geometry parameters and material properties:

$$L = 100\ \mathrm{nm},\ \ k = 315\ \mathrm{W\,m^{-1}\,K^{-1}},\ \ \alpha = 1.2\times10^{-4}\ \mathrm{m^2\,s^{-1}},$$
$$\tau_q = 8.5\times10^{-12}\ \mathrm{s},\ \ \tau_T = 90\times10^{-12}\ \mathrm{s}.$$

Fig. 3 shows the comparison of the temperature variation θ between the present numerical results and the analytical solutions given by Ref. [7] along the x direction at various t values. It is noticeable that the present numerical results agree well with the analytical solutions. The temperature variation θ decreases with the increase of x in Fig. 3. Since the laser heating is applied at the left boundary, θ initially increases very rapidly and then decreases with time near the left boundary due to the characteristics of hyperbolic heat conduction. In contrast to the thermal wave model in hyperbolic heat conduction ($\tau_T = 0$), the existence of the τ_T enlarges the penetration depth of thermal signal and destroys the waveforms as shown in Fig. 3. This implies that the pulse thermal disturbance can be dissipated by the diffusive effect of τ_T. However, some wave propagation features can still be observed in Fig. 3.

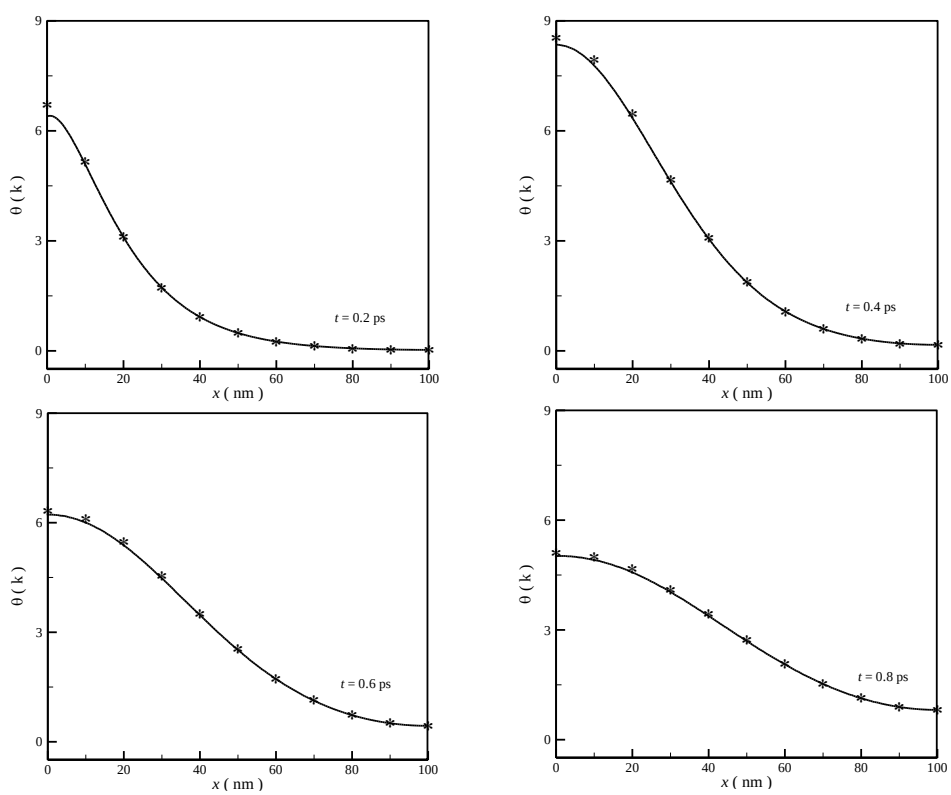

Fig. 3. Comparison of $\theta(x,t)$ between the present results and the analytical solutions [7] at various t values; the solid line refers to the analytical solutions and the star to the present results

Fig. 4 demonstrates the variation of temperature with time in the gold film at four different locations. The temperature variation in Fig. 4 is depicted for duration of 6 ps. Again, the results by the present numerical method are in very good agreement with those of the analytical values in Ref. [7]. The temperature variation at all locations initially increases and then continually decreases with time. The highest rate of decrease is at the left boundary due to the high heat losses at that location.

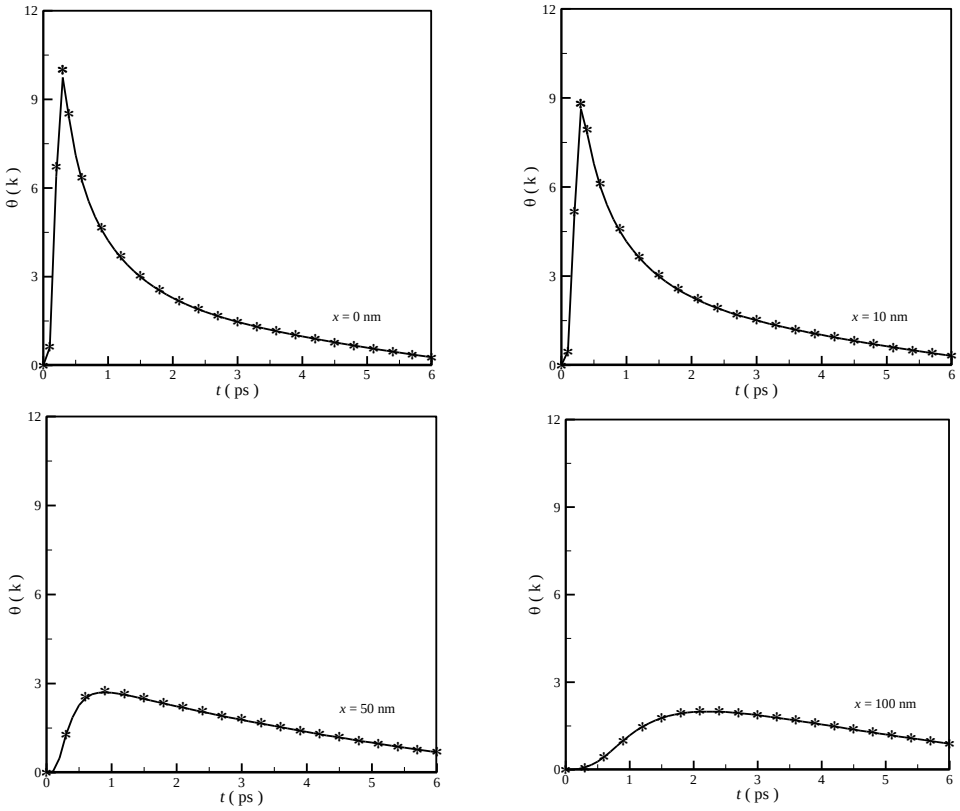

Fig. 4. Comparison of $\theta(x,t)$ between the present results and the analytical solutions [7] at different positions; the solid line refers to the analytical solutions and the star to the present results

With the correctness of the numerical procedure been proved, the effects of τ_q and τ_T on temperature variation can be investigated. To illustrate the effect of τ_q on temperature variation, Fig. 5 depicts the variation of temperature along the *x* direction at various values of τ_q for $\tau_T = 90$ ps and *t* = 0.4 ps. It can be noted in Fig. 5 that the wave front is more observable in the case of larger τ_q. Since τ_q is normally interpreted as non-zero time that accounts for the effect of "thermal inertia" [11], τ_q is responsible for the delay in establishing heat flux and associated conduction through the medium. This delay tends to induce thermal waves with sharp wave-fronts separating heated and unheated zones in the metal film.

To investigate the effect of τ_T on temperature variation, Fig. 6 shows the temperature variation along the *x* direction at various τ_T values, given $\tau_q = 8.5$ ps and *t* = 0.4 ps. It can be seen in Fig. 6 that the wave front is less noticeable in the case of larger τ_T. Since τ_T can be interpreted as non-zero time that accounts for the effect of "microstructural interaction" [11], τ_T is the delay in establishing the temperature gradient across the medium during which conduction occurs through its microstructures. As a result, τ_T makes the sharp wave-fronts caused by τ_q smoother by promoting conduction, resulting in non-Fourier diffusion-like conduction. This can be seen in Fig. 6 that increasing τ_T "flattens" the temperature profiles. Since

each profile in Fig. 6 reflects the same amount of energy provided by the laser heating, as τ_T increases, profiles extend deeper into the metal film. They must become flattened to reflect the same laser energy content.

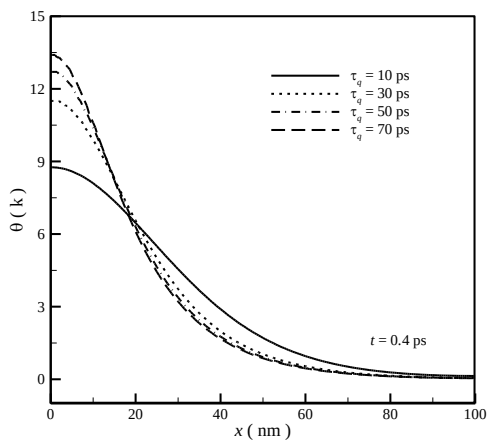

Fig. 5. Temperature variation $\theta(x,t)$ with x various τ_q values in the gold film for τ_T = 90 ps and t = 0.4 ps

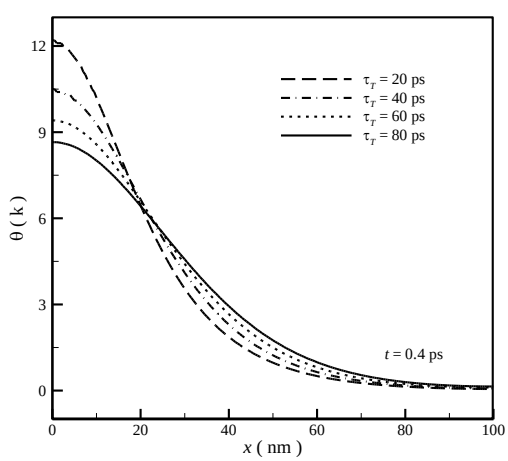

Fig. 6. Temperature variation $\theta(x,t)$ with x at at various τ_T values in the gold film for τ_q =8.5 ps and t = 0.4 ps

5. Conclusion

The present study numerically analyzes the hyperbolic heat conduction problem of short-pulse laser heating on a thin metal film using the DPL model with constant phase lags by a hybrid numerical scheme. The numerical scheme involves the hybrid application of the Laplace transform and control volume methods in conjunction with hyperbolic shape functions. Comparison between the numerical results and the analytic solution for a short-pulse laser heating with the Gaussian temporal profile evidences the accuracy of the present numerical results. Effect of different phase lags values of the heat flux and the temperature gradient on the behavior of heat transfer is also investigated. The results indicate that τ_q is responsible for the delay in establishing heat flux and associated conduction through the medium. On the contrary, the existence of τ_T destroys the waveforms and enlarges the penetration depth of thermal signal.

Acknowledgements

This work was supported by the Ministry of Science and Technology, Taiwan, Republic of China, under the grant number MOST 103-2221-E-168-026.

References

Al-Nimr, M.A., & Arpaci, V.S. (1999). Picosecond Thermal Pulses In Thin Metal Films. *J. Appl. Phys.*, 85, 2517–2521.

Meijer, J., Du, K., Gillner, A., Hoffmann, D., Kovalenko, V.S., Masuzawa, T., Ostendorf, A., Poprawe, R., & Schulz, W. (2002). Laser Machining By Short And Ultrashort Pulses, State Of The Art And New Opportunities In The Age Of The Photons. *Annals of the CIRP*, 51, 531–652.

Tzou, D.Y. (1996). *Macro- To Microscale Heat Transfer: The Lagging Behavior*. Washington, DC: Taylor and Francis

Tzou, D.Y. (1995). Experimental Support For The Lagging Response In Heat Propagation. *J. Thermophys. Heat Transfer*, 9, 686–693.

Ordóñez-Miranda, J., & Alvarado-Gil, J.J. (2010). Exact Solution Of The Dual-Phase-Lag Heat Conduction Model For A One-Dimensional System Excited With A Periodic Heat Source. *Mech. Res. Commun.*, 37, 276–281.

Liu, K.C., & Chen, H.T. (2010). Investigation For The Dual Phase Lag Behavior Of Bio-Heat Transfer. *Int. J. Therm. Sci.*, 49, 1138–1146.

Ramadan, K., Tyfour, W.R., & Al-Nimr, M.A. (2009). On The Analysis Of Short-Pulse Laser Heating Of Metals Using The Dual Phase Lag Heat Conduction Model. *ASME J. Heat Transfer*, 131, 111301-1–111301-7.

Liu, K.C. (2006). Numerical Simulation For Non-Linear Thermal Wave. *Appl. Math. Comput.*, 175, 1385–1399.

Liu, K.C., Lin, C.N., & Wang, J.S. (2005). Numerical Solutions For The Hyperbolic Heat Conduction Problems In A Layered Solid Cylinder With Radiation Surface. *Appl. Math. Comput.*, 164, 805–820.

Yang, Y.C., Lee, H.L., Hsu, J.C., & Chu, S.S. (2008). Thermal Stresses In Multilayer Gun Barrel With Interlayer Thermal Contact Resistance. *J. Therm. Stresses*, 31624–637.

Antaki, P.J. (1998). Solution For Non-Fourier Dual Phase Lag Heat Conduction In A Semi-Infinite Slab With Surface Heat Flux. *Int. J. Heat Mass Transfer*, 41, 2253–2258.